Modeling Side-Stream Enhanced Biological Phosphorus Removal (S2EBPR) System Using Agent-based Model with Adaptive Maintenance, Decay and TCA Metabolism

Guangyu Li [1], Nicholas B. Tooker [1], Dongqi Wang [1,2], Varun Srinivasan [1], James L. Barnard [3], Andrew Russell [4], Imre Takacs [5], Charles Bott [6], Paul Dobrowski [7], Annalisa Onnis-Hayden [1], and April Z. Gu [8,*]

[1] Department of Civil & Environmental Engineering, Northeastern University, Boston, MA, United States

[2] Department of Municipal and Environmental Engineering, Xi'an University of Technology, Xi'an, Shaanxi, China

[3] Black & Veatch, Kansas City, MO, United States

[4] South Cary Water Reclamation Facility, Apex, NC, United States

[5] Dynamita, Nyons, France

[6] Hampton Roads Sanitation District, Virginia Beach, VA, 23454, United States

[7] Woodard & Curran, Inc., CT, 06082, United States

[8] School of Civil and Environmental Engineering, Cornell University, Ithaca, NY, United States

KEYWORDS: EBPR, S2EBPR, Agent-based modeling, Cell maintenance, Cell decay, Glycolysis-TCA pathway switch

ABSTRACT

Side-stream enhanced biological phosphorus removal process (S2EBPR) refers to modified EBPR configurations that have been demonstrated to improve the performance stability and offer a suite of advantages compared to conventional EBPR design. Design and optimization of S2EBPR requires modification of the current EBPR models that were not able to fully reflect the metabolic functions of and competition between the PAOs and GAOs under extended anaerobic conditions as in the S2EBPR conditions. In this study, we proposed and validated an improved iEBPR model for simulating PAO and GAO competition that incorporated heterogeneity and versatility in PAO sequential polymer usage, staged maintenance-decay and glycolysis-TCA pathway shifts. The iEBPR model was first calibrated against a bulk batch test experimental data. The improved iEBPR model performed better than the previous EBPR model for predicting the soluble orthoP, ammonia, biomass glycogen and PHA temporal profiles in a batch starvation testing under prolong anaerobic conditions. We further validated the model with another independent set of batch anaerobic batch testing data that included high-resolution cellular and population-level intracellular polymers measurements enabled by single-cell Raman microspectroscopy technique. The model accurately predicted the temporal changes in the intracellular polymers at cellular and population levels within PAOs and GAOs, further confirmed the proposed mechanism of sequential polymer utilization, and polymer availability-dependent and staged maintenance and decay in PAOs. These results indicate that under extended anaerobic phases as in S2EBPR, the PAOs may gain competitive advantage over GAOs due to the possession of multiple intracellular polymers and the adaptive switching of the anaerobic metabolic pathways that consequently lead to the later and slower decay in PAOs than GAOs. The iEBPR model can be applied to facilitate and optimize the

design and operations of S2EBPR for more reliable nutrient removal and recovery from wastewater.

INTRODUCTION

Enhanced biological phosphorus removal (EBPR) process has been recommended as a promising strategy to achieve sustainable wastewater P removal and simultaneous P recovery [1]. Current EBPR systems are driven by and engineered to favor a key functional group, phosphate-accumulating organisms (PAOs) such as the *Candidatus Accumulibacter phosphatis*, which is the most commonly found PAO in EBPR systems. Glycogen-accumulating organisms (GAOs) are often found to coexist with PAOs but lacking polyP metabolism. They have similar glycogen-based VFA-PHA metabolism [2,3] concerned to be niche VFA competitor with PAOs but have limited contribution to P removal performance. PAO-GAO competition could be a critical factor in EBPR performance and is kinetically affected by various factors including pH, temperature and hydraulic retention time (HRT) etc. [4–8]. Meanwhile, the existence of GAOs does not necessarily deteriorate EBPR performance as long as PAOs are kinetically favored [1,9,10].

The performance stability of EBPR has been a concern for its wide implementation in practice and its sustainability advantages are often offset by the needs to have chemicals standby for ensuring reliable P removal performance to consistently meet compliance [1,9,11]. Many facilities still suffer from inconsistent performance with unpredicted upsets, particularly for those with relatively weak influent readily biodegradable COD (rbCOD) [1,5,6,12]. An emerging technology that has been demonstrated to successfully address this common stability challenge is side-stream RAS and mixed liquor hydrolysis/fermentation-based side-stream EBPR (S2EBPR) [1,9,11,13–18]. S2EBPR refers to modified EBPR configurations that include diversion of a portion of RAS or anaerobic

mixed liquor to a side-stream reactor, where simultaneous VFA production via sludge hydrolysis and fermentation and PAO activity-related P release and carbon uptake occur. Compared to conventional EBPR design, the S2EBPR offers a suite of advantages including influent-carbon independent condition for PAO enrichment that eliminates the influences of fluctuating influent loads, more controllable lower-redox environment with more complex VFA composition that provides more favorable selection of PAOs over GAOs, flexible implementation configurations and potential reduction of carbon footprint and denitrification enhancement by diverting more influent carbon to denitrification [1,9,11,19–22]..

While full-scale processes demonstrated the potential promises and advantages of S2EBPR [9,11,13–18], existing knowledge gaps in fundamental understanding of the biochemical mechanisms and microbial ecology involved in S2EBPR hampers its wider application and implementation. Design and optimization of S2EBPR requires adequate EBPR models that can capture the underlying key mechanisms involved in the S2EBPR such as the VFA production via hydrolysis and fermentation, and PAO and GAO competition in the extended-anaerobic side-stream reactor. A few recent modeling efforts failed to predict either this competitive advantage or the performance superiority observed in S2EBPR systems compared to the conventional EBPR systems [23,24]. This suggested that there are still critical aspects in the current EBPR models that cannot reflect the metabolic functions of and competition between the PAOs and GAOs under the S2EBPR conditions, such as cell maintenance, biomass decay, the utilization of intracellular polymers, and PAO/GAO metabolic versatility under the prolonged anaerobic condition [25,26].

PAOs' cell maintenance is a hypothesized metabolic process from the observation of their steady-state and consistent intracellular glycogen and polyP degradation that are independent of their

EBPR-related metabolic activities such as PHA synthesis [2,4,24,27–31]. Studies showed that PAOs continued consuming their intracellular glycogen and polyP both during short-term (about 10 hrs) [4,27,28] and long-term (≥5 days) [29] anaerobic treatments without external VFA supply and they were not coupled with EBPR-associated VFA uptake and storage. Similar experimental evidence was observed for GAOs who had cell maintenance during both short-term [2,24,30,31] and long-term [29] anaerobic conditions solely based on glycogen. The possession and ability to utilize both polyP and glycogen depending on their availability for maintenance energy derivation by PAOs led to the seemingly inconsistent observations of polymer utilization priority under the similar anaerobic conditions. This highlighted the importance of the more pronounced effects of anaerobic metabolic versatility of PAOs, particularly under extended anaerobic condition such as those in S2EBPRs [32,33]. However, in current EBPR models, PAO cell maintenance is often approximated by either first-order decay of polyP and/or glycogen (e.g. ASM2 and ASM3+BioP [34]), or polyP-only cleavage (e.g. Barker&Dold and UCTPHO+ [35,36]) without accounting for glycogen. Recent studies attempted sequential polymer usage strategy [26,37,38] to mitigate the overestimation of polymer consumption encountered in traditional EBPR models that use first-order decay (e.g. ASM2 and ASM3+BioP [34]) and polyP cleavage (e.g. Barker&Dold and UCTPHO+ [35,36], which ignores glycogen). More accurate modeling of the cell maintenance processes in PAOs and GAOs under the unique and prolonged anaerobic conditions can improve the modeling efficiency of S2EBPR systems[39]. Li et al. (2018; 2020) and Santos et al. (2020) further extended the cell maintenance to the "survival" hypothesis, in which maintenance precedes biomass decay, to explain the observed low PAO/GAO decay rate in comparison to other heterotrophic organisms under anaerobic conditions [26,38,40]. However, with complex microbial communities, current population-level

models still cannot estimate the effect of mixture phenotypes and non-uniformity in polymer distributions [8,41] and capture the detailed PAO-GAO competition at phenotype/cell group level.

The most debated aspect related to the Accumulibacter's anaerobic metabolism is the source of reducing power (NAD(P)H). In early studies, this source was deduced to be exclusively supported by glycolysis (referred to as Mino model) [42] or solely supported by tricarboxylic acid (TCA) cycle (referred to as Comeau-Wentzel model) [27,43]. Both models were supported by additional experiments [4,44], while some others suggested potential coexistence and simultaneous contribution to t NAD(P)H production [45–48]. A switch between these pathways may occur and was hypothesized to be related with intracellular polymer availability or depletion [25,45,48,49]. Another critical discussion on the anaerobic operation of complete TCA proposed that the oxidation of succinate thermodynamically is unfavorable which relies on external electron acceptors (TEAs) [28]. Four potential mechanisms have been proposed that either bypass this oxidation step or employ alternative ways to sink the electrons, namely succinate-propionate shunt [50], partial reductive TCA cycle [50–52], glyoxylate shunt [47,53,54] or proton motive force-driven quinol-NAD(P)$^+$ reductase [55]. Each proposed theoretical pathway was supported by physiological, genomics, transcriptomics or proteomics evidences, and exhibits different stoichiometry on glycogen, polyP, VFAs, PHAs and CO_2 release. This metabolic versatility may help explain the wide range of stoichiometry observed in a variety of full-scale studies [25]. Santos et al. (2020) introduced the pathway switching mechanism to better reproduce this complicated, flexible metabolic network [38]. However, traditional EBPR models cannot simulate such pathway shift effects as the essential yield coefficients was kept constant during the simulation after calibration, nor distinguish between coexisting PAO phenotypes with different glycolysis and TCA cycle operations.

132 In this study, with the long-term goal to better predict the S2EBPR processes, we proposed and
133 validated an improved model for PAO and GAO competition under extended anaerobic conditions
134 that incorporated heterogeneity and versatility in PAO sequential polymer usage, staged
135 maintenance-decay and glycolysis-TCA pathway shifts. More importantly, we further calibrated
136 and verified the model by leveraging the power of single-cell Raman microspectroscopy
137 technology that enabled cellular-level quantification of intracellular dynamics under various
138 conditions [8,41,56]. The model was first calibrated using a previously published 8-day anaerobic
139 starvation testing in PAO-enriched (85% as PAO) EBPR batch reactor [33]. Then the calibrated
140 model was validated using an independent 72-hour continuous anaerobic incubation batch test with
141 sludge from a full-scale S2EBPR system. The model outperformed the previous model in
142 predicting the experimentally observed trends of intracellular polymer biomass content under
143 anaerobic conditions and was proven to be more effective in simulating PAO/GAO maintenance
144 behavior under those extended anaerobic conditions than conventional models. The proposed
145 mechanism can be incorporated into industrial EBPR models to more accurately reveal the overall
146 EBPR performance and PAO/GAO competitive dynamics as observed in S2EBPR systems.

147 **METHODOLOGY**

148 **Agent-based EBPR model structure**

149 An agent-based EBPR model (named as iEBPR) was developed based on the model (named as
150 iAlgae) developed by Bucci et al. (2012) [56]. In this study, three population groups are included,
151 namely PAOs, GAOs and OHOs (ordinary heterotrophic organisms, accounting for all non-
152 PAO/GAO biomasses). The agent-based approach splits each biomass category in 10,000 agents

153 (representing cell groups with phenotypic heterogeneity) with randomly seeded polymer contents
154 and kinetic parameters.

155 The metabolic framework and structure of iAlgae were developed based on the International Water
156 Association's Activated Sludge Model v2 (ASM2) that includes Accumulibacter-PAOs and OHOs
157 [34]. A third organism type, namely Competibacter-like GAO, is added to the new model based on
158 the current understanding of the main cell activities of GAOs including anaerobic VFA-uptake,
159 PHA synthesis and aerobic biomass growth PHA-degradation and glycogen-accumulation [2,24,31].
160 At this stage, the iAlgae uses only acetate to represent all VFA species without differentiating
161 various VFAs such as propionate etc. Similarly, PHB was chosen to represent PHA as in similar
162 modelling study [38]. As we focused on PAO-GAO competition under extended anaerobic condition,
163 denitrifiers, nitrifiers and other anoxic-related metabolisms are not included in this modeled. The
164 hydrolysis and fermentation of inert organic matter was considered not bottlenecking the rbCOD
165 generation and was modeled as instant transformation to the final VFA product. All modeled
166 processes for Accumulibacter-PAOs, Competibacter-GAOs and OHOs are shown in **Table S1-3**
167 with Gujer matrices.

168 **Agent-level energy derivation for cell maintenance and decay with polymer-availability**
169 **dependence**

170 Similar to previous studies [37,38], sequential polymer usage and staged cell maintenance-decay was
171 incorporated into the model however at agent-level. This process replaces the first-order decay
172 calculation in ASM2. Specifically, this was modeled in two steps below.

173 ***Cell maintenance and sequential polymer usage.*** Each PAO and GAO agent possesses a
174 parameter called targeted cell-maintenance rate, denoted as m^{ATP}, expressed in mol-ATP/(C-mol
175 biomass.hr). The unit was further converted to fit the unit specifications in our model (mg polyP-
176 P and mg glycogen-COD) based on known stoichiometry and yield coefficients reported in the
177 previous studies [2,4,31,33]. Its proto-value was experimentally determined in previous studies [2,7,31]. In
178 agent-based modeling, the value may vary based between agents to emulate the metabolic
179 heterogeneity between cells and phenotypes. Each PAO and GAO agent will attempt to fulfill their
180 own cell-maintenance target according on their local intracellular polymer availability.
181 Specifically, GAOs will generate ATP via the previously proposed stoichiometry [2,31] when
182 glycogen is available. For PAO cells, the same glycogen-based stoichiometry was used [33] as well
183 as the stoichiometry of ATP production from polyP cleavage [4]. In addition, extra mechanism must
184 be introduced to allocate the contributions from both glycogen and polyP based on the agent
185 phenotype of preferences. For polyP-preferred agents, this was calculated as

186 $$r_{polyP} = M_{polyP} m^{ATP}$$

187 $$r_{glycogen} = M_{glycogen}\left(m^{ATP} - r_{polyP}\right),$$

188 while for glycogen-preferred agents, this was calculated as

189 $$r_{glycogen} = M_{glycogen} m^{ATP}$$

190 $$r_{polyP} = M_{polyP}\left(m^{ATP} - r_{glycogen}\right)$$

191 instead. Where: r_{polyP} and $r_{glycogen}$ are the real-time ATP generation rate from the respective
192 polymer; m^{ATP} is the target cell-maintenance rate; M_{polyP} and $M_{glycogen}$ are Monod functions
193 scaling the production rate based on the availability of the respective polymer. It is important to
194 note that this calculation strategy can be easily extended to calculation with more than two
195 polymers in sequential preferences. This approach simulates the observed sequential polymer
196 usage in various studies [29,32,33]. Unlike other models reported in the literature where the sequence
197 of polymer usages is pre-chosen [37,38], we set the polymer preference order as an adjustable
198 parameter to simulate the PAO metabolic versatility and observations with inconsistent
199 prioritization [32,33].

200 ***Sequential and linked cell maintenance and decay.*** Previous EBPR models considered the cell
201 decay as an intrinsic process at a constant specific rate i.e., first-order decay. A number of studies
202 have showed evidence of accelerated biomass decay after depletion of their intracellular polymers,
203 implying a linkage between these two processes [29,33]. To simulate this linkage, we first calculated
204 the combined ATP production from all involved polymers in cell maintenance, then compared it
205 with the target cell-maintenance rate (denoted as m^{ATP}) [26]. If the production is short from the
206 target, the proportion of the shortage was used as a switching function to scale the actual biomass
207 decay rate, namely,

208 $$b_r = b_{max}\left(1 - \frac{r^{ATP}}{m^{ATP}}\right),$$

209 where: b_r is the actual specific decay rate; b_{max} is the maximum specific decay rate; r^{ATP} is the
210 combined ATP production from cell maintenance processes. The decayed biomass then
211 proportionally regenerates as VFA (rbCOD) based on the empirical PAO/GAO biomass formula

212 $CH_{1.93}O_{0.53}N_{0.2}$ [2]. This calculation states a "maintenance precedes decay" mechanism that PAO
213 and GAO biomasses are able to suffer no biomass decay when they have ample polymer for cell
214 maintenance. In other words, the cell maintenance was hypothesized as a "survival" strategy for
215 PAO and GAO cells under anaerobic conditions [38].

216 **Glycolysis and TCA cycle pathway switching**

217 As discussed previously, current knowledge suggests that PAOs can use both glycolysis and TCA
218 cycle to generate the reducing power needed in PHA synthesis. The major difference between
219 glycolysis-oriented and TCA-oriented metabolism (including various TCA-cycle operation
220 patterns) is glycogen dependency [45,47]. Namely, PHA synthesis solely supported by TCA cycle
221 will remain operatable after glycogen depletion [25,45]. Dominant use, or a combined employment at
222 various degrees of these two pathways have been evidenced and discussed [20,27,28,43–48,57]. In this
223 study, we simplify the metabolic network to two principal stoichiometry models, namely sole
224 glycolysis (Mino model) [28,57] and full TCA cycle (Comeau-Wentzel model) [27,43], which are both
225 well established, and widely adopted in EBPR modeling applications. To simulate the various
226 degrees of deployment of these two pathways, the final stoichiometry was calculated as their
227 weighted mixture, where the weights of respective pathway was calculated from the availability
228 of respective polymers. This is considered as a common approach which was also used by previous
229 studies in both stoichiometric analysis [45,47] and modelling [37,38]. Therefore, the change of polymer
230 availability during simulation will also change the weight ratio between pathways, simulating the
231 polymer-dependent pathway shift. However, this calculation implies that PAOs much rely on
232 polyP in PHA synthesis and disallows them shifting to GAO-like metabolism; though it is not
233 necessarily true in reality [25,58]. In addition, to account for the PAO phenotypes that may strictly

234 require glycogen in PHA synthesis [28,50], we also included a second type of PAO agents that cannot
235 switch to TCA-oriented metabolism when glycogen is depleted. This multi-phenotype feature
236 within a single biomass category is exclusive to agent-based modelling.

237 **Agent pool initialization and discrete-time simulation**

238 All agents were generated by randomizing the cellular states and kinetic traits via individual
239 seeding distributions, which can be calibrated with observation datasets revealing in-species
240 heterogeneities. Only the cellular biomass, polymer storage, rates and affinity-related traits are
241 randomized; stoichiometric coefficients are considered as pre-determined constants as they can be
242 theoretically determined or empirically justified. The number of agents is an important parameter
243 in agent-based modeling. A larger agent pool trends to have generated traits statistically better
244 approximate the pre-defined seeding distributions, however, will proportionally increase the
245 computational load. We found that using 1,000-10,000 agents per biomass was a good
246 compromise. In addition, we used discrete-time simulation approach with all agents updated
247 synchronously at each simulated time step.

248 **Model Calibration**

249 Simulation of the PAO and GAO competition under extended anaerobic conditions via the
250 modified agent-based EBPR model (iEBPR) was first calibrated with an independent set of data
251 retrieved from a previous 8-day anaerobic starvation study in a lab-scale Accumulibacter-enriched
252 (reported abundance of ~85%) EBPR system [33]. The initial content of glycogen and PHA was
253 acquired from the published data with the polyP estimated by assuming a full cleavage and release
254 at the end of the experimental period. Anaerobic kinetic parameters of PAOs and GAOs are
255 calibrated. Gradient descent technique is used as automated calibration method. For detail, the

256 geometric mean of root mean square errors (RMSEs) calculated from predicted and observed
257 temporal profiles of PHA, glycogen, orthophosphate and MLVSS was used as the loss function.
258 The gradient descent algorithm hence could start from an arbitrary initial parameter set then
259 iteratively adjust those parameter values in the direction where the loss function reduces the fastest,
260 until hitting a local minimum. The global optimum was attempted by repeating the above process
261 for 10,000 times; then the final parameter set corresponds to the least loss was selected as the
262 calibration result. Yield coefficients used the values from previous studies and ASM2 model
263 defaults with unit conversions if necessary [2,7,59]. **Table S4-6** shows the final parameter set for
264 PAOs and OHOs respectively, and unit conversions are shown in **Note S7**.

265 **Comparison of model results with cellular-level experimental observations via single-cell**
266 **Raman microspectroscopy**

267 Previous studied proposed single-cell Raman spectroscopy (SCRS) to be a promising technology
268 in estimating the glycogen, PHA and polyP in individual cells, to further reveal the polymer
269 distributions at both cellular and population levels. [41,60–62]. This phenotypic survey data is
270 comparable with the polymer distribution predicted by agent-based modelling [56].

271 ***SCRS dataset acquisition.*** An SCRS dataset was first acquired for each individually sludge sample
272 based on the method detailed in previous studies [1,8,41]. Briefly, 1 mL of MLSS was washed twice
273 with 0.9% (w/v) NaCl solution and homogenized by passing in and out of a 26-gauge needle and
274 syringe for at least 20 times to obtain uniform distribution of cells, as described previously. Then
275 6-8 drops of the disrupted sample were spread and dried on aluminum-coated slides (EMF Corp.,
276 Ithaca, US). After that, the slide was dipped into ice-cold Milli-Q water several times to remove

277 salt particles, and dried by filtered nitrogen gas. For each sample, Raman spectra for at least 40
278 single cells were acquired using a multiline confocal Raman spectrometer (LabRam HR Evolution,
279 Horiba Jobin Yvon, Kyoto, Japan) configured with a 532 nm Nd:YAG laser and a 600 gr/mm
280 grating. A 100× long working distance objective with a numerical aperture (NA) of 0.9 and a
281 working distance of 0.21 mm was used to observe and collect Raman signal from single cells. The
282 acquisition time for each individual spectrum was 20 seconds per cell and the laser power was set
283 to 10%. Spectra were collected with scan from 400 cm^{-1} to 1800 cm^{-1}.

284 ***SCRS data processing.*** Raman spectra processing and polymer relative abundance calculation
285 were detailed by Gu et al. (2018)[1]. All Raman spectra were processed using cosmic spike removal,
286 smoothing, background subtraction and baseline correction using LabSpec 6 software (Horiba
287 Jobin Yvon, Kyoto, Japan). Quality control was conducted by excluding the spectra showing
288 unexpected signals (damaged) or low SNR, or lack of major characteristic peaks from bacterial
289 components such as phenylalanine (~1002 cm^{-1}) and amide I (~1657 cm^{-1}). The candidate PAO
290 and GAO populations were quantified based on the different combinations of intracellular
291 polymeric inclusions, including poly-P (band at 690-700 cm^{-1} for P-O-P vibrations and band at
292 1168-1177 cm^{-1} for PO_2^- stretching band), PHAs (bands at ~434 cm^{-1},~839 cm^{-1}, and ~1723 cm^{-1}),
293 and glycogen (bands at ~480 cm^{-1},~852 cm^{-1}, and ~938 cm^{-1}), as described previously [62]. The
294 relative content of poly-P, PHAs, and glycogen in each candidate PAO and GAO cell were
295 evaluated based on the intensity of the bands at 1168-1177 cm^{-1}, ~1723 cm^{-1}, and ~480 cm^{-1},
296 respectively (normalized against the intensity of the amide I band). The polymer distribution in
297 PAO and GAO biomass was then estimated based on the polymer relative abundances within PAO
298 and GAO candidate cells collected in each sample respectively.

299 **RESULTS AND DISCUSSION**

300 **Model calibration with batch testing results**

301 The model was calibrated against the temporal profile of orthophosphate and residual ammonia
302 concentration, intracellular glycogen and PHA storage (Figure 1). The ammonia concentration was
303 calculated from the modeled biomass decay in the same method proposed by Lu et al. (2007) [33].
304 Figure 1 shows the comparison of the experimental data with the predicted orthoP, ammonia,
305 glycogen and PHA temporal profiles by the improved model and previous agent-based model
306 iEBPR (without the staged maintenance-decay and sequential polymer utilization for cell
307 maintenance). The improved iEBPR model performed quantitatively better than the previous
308 iAlgea model (Table 1). Particularly, note that the revised model reflects the "S-shape" of the
309 orthoP profile indicating a first acceleration and then deceleration of polyP degradation. While the
310 previous model predicted a deviated profile without this acceleration. The glycogen profiles are
311 predicted with similar trend from both models; while only the improved model predicted the
312 increase in polyP-origin ATP production from Day 1-3 resulted from the sequential polymer
313 utilization that shifted from glycogen-dependent to poly-P dominant. Based on these experimental
314 observations, the 8-day anaerobic starvation could be divided into four phases: Day 0-1: Glycogen
315 degradation phase signatured by fast glycogen reservoir depletion within the first day,
316 accompanied by corresponding PHA formation; Day 1-2: Continuous glycogen degradation but
317 with a slower rate until the end of Day 2; the PHA formation rate was also lowered concurrently.
318 The glycogen content was still above detection limit after this stage, but no significant change was
319 observed afterwards. Meanwhile, there was minimal decay of biomass (indicated by releasing
320 residual ammonia); Day 2-4: PolyP degradation phase accompanied with increasing residual

orthoP concentration and slowly increasing residual ammonia implying no significant cell decay; Day 4-8: Decelerating releasing rate of phosphate indicated the degradation of polyP was slowing down, which was accompanied with detectable increase in the residual ammonia signifying accelerated cell biomass decay.

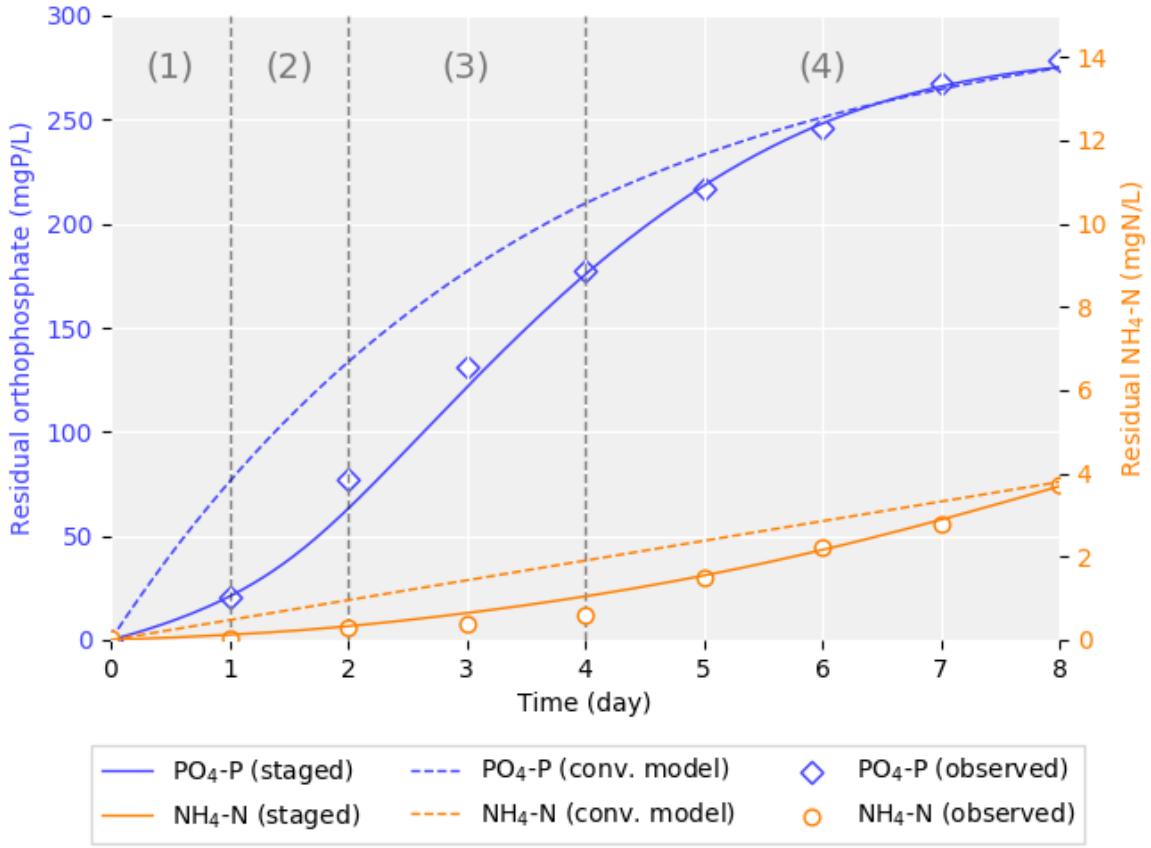

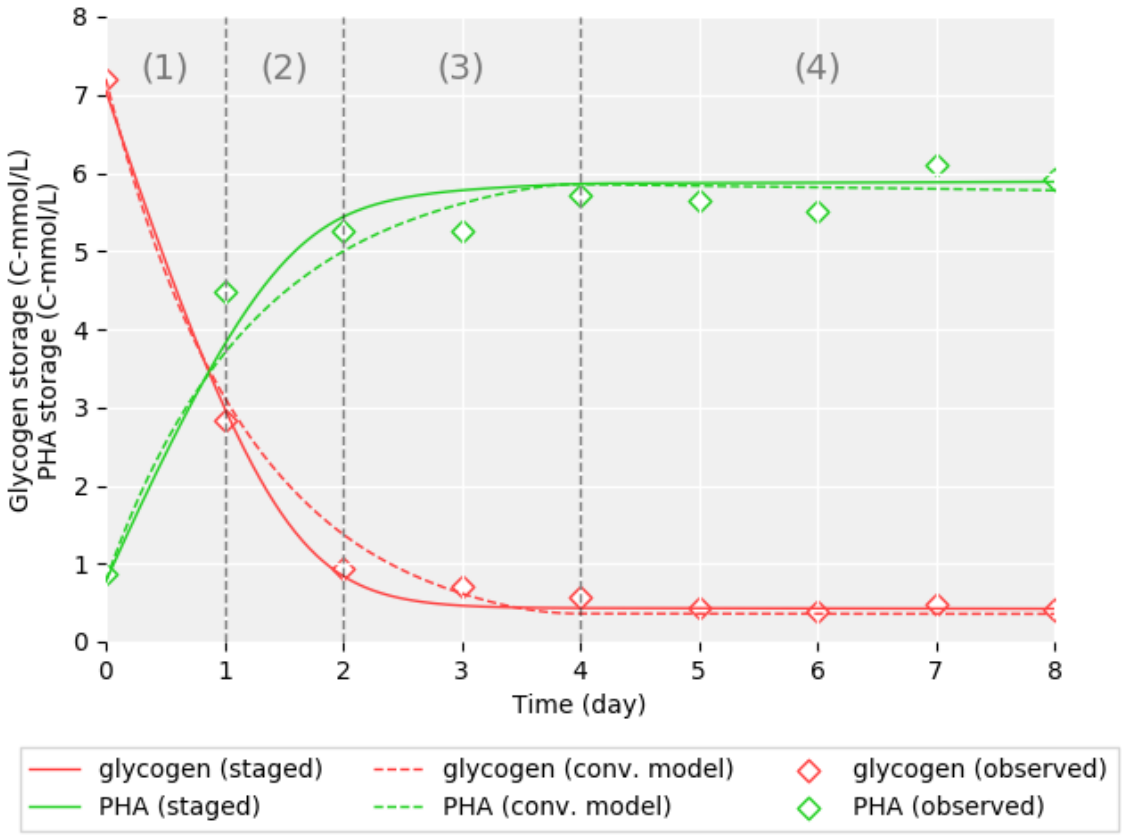

Figure 1. Model calibration by comparing the simulations results via the iEBPR model against the temporal experimentally measured profiles of PO_4-P, ammonia, intracellular glycogen and PHA in an acetate-fed lab-scale EBPR system with approximately 85% Accumulibacter-PAOs during an 8-day anaerobic starvation batch test (Lu et al. (2007)). Top shows the residual orthophosphate and ammonia-nitrogen profiles, and the bottom shows intracellular glycogen and PHA. Results were also compared with the simulation results from the previous iAlgae model that uses first-order polymer decay. Number (1)-(4) indicate the four differential stages observed during the batch test: (1) rapid glycogen degradation; (2) transit stage with decreasing glycogen depletion rate and increasing polyP hydrolysis rate; (3) polyP degradation with glycogen being depleted; and (4) polyP depleting stage with on-set of significant cell decay (indicated by the increased release of residual ammonia).

Notably, the calibrated PAO cell maintenance rate was 2.1×10^{-3} mol ATP/(C-mol VSS·hr), which resided in the range shown in Table 1. The model calibration suggested that only a very small or portion of PAOs (< 1%) can utilize TCA cycle. This agreed with the results found in original experiment where no significant PHA formation was observed after glycogen depletion [33].

342 Table 1. Modelling accuracy (RMSE) comparison between iEBPR and iAlgae. Observation data acquired
343 from an 8-day anaerobic starvation test of an acetate-fed PAO-enriched (about 85% as PAOs) lab-scale
344 sludge by Lu et al. (2007).

Model	RMSE			
	PO_4-P mgP/L	NH_4^+-N mgN/L	PHA C-mol/L	Glycogen C-mol/L
iEBPR (Improved with staged maintenance-decay, sequential anaerobic maintenance polymer usage and glycolysis-TCA pathway switching, this study)	5.98	0.18	0.34	0.12
iAlgae-ASM2[34,56]	33.0	1.08	0.34	0.19

345

346 **Improved accuracy in predicting PAOs' competitive advantage**

347 Comparing to the Lu et al. (2007)'s original experimental data, both the improved iEBPR and the
348 conventional iAlgea models predicted a high-rate glycogen utilization in the first stage day, while,
349 only the improved model that incorporated staged maintenance and decay was able to predict the
350 accelerated polyP degradation upon the depletion of glycogen as observed in the stage 2 and 3.
351 This suggested that Accumulibacter-like PAOs biomass seemed to prefer the utilization of
352 glycogen over poly-P as energy source when both are available as they are consumed first and
353 fulfilled the theoretical cell-maintenance ATP requirements. This was accompanied by the
354 transition from glycogen-oriented towards a polyP-oriented cell maintenance. Figure 2 shows the
355 calculated distribution of ATP production originated from the glycogen versus those from polyP.

356 Note that the previous model (iAlgae) that uses the first-order decay to approximate cell
357 maintenance failed to reflect the observed transition from dominantly glycogen-dependent ATP

production to a stage with accelerated polyP utilization upon the depletion of glycogen (Figure 1 and Figure 2). The overestimation of PAOs' polyP consumption under anaerobic conditions within the first 24 hrs (more relevant to the anaerobic condition in full-scale EBPR systems) hence may underestimate the PAOs' competition advantage under anaerobic conditions. This overestimated polyP cleavage caused the traditional model to over-predict about 56 mgP/L P release than the observation at the end of Day 2 Figure 1 (top). The incorporation of the staged-maintenance and decay with sequential polymer utilization better predicted PAOs biomass decay kinetics under anaerobic conditions comparing to conventional model.

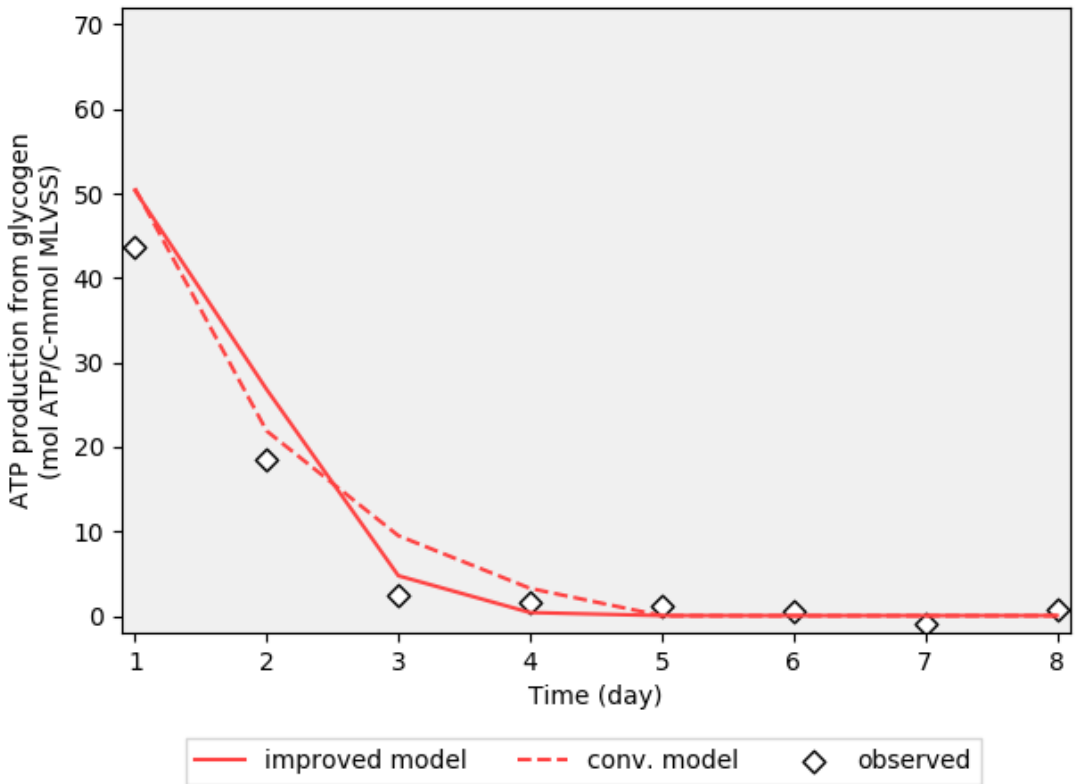

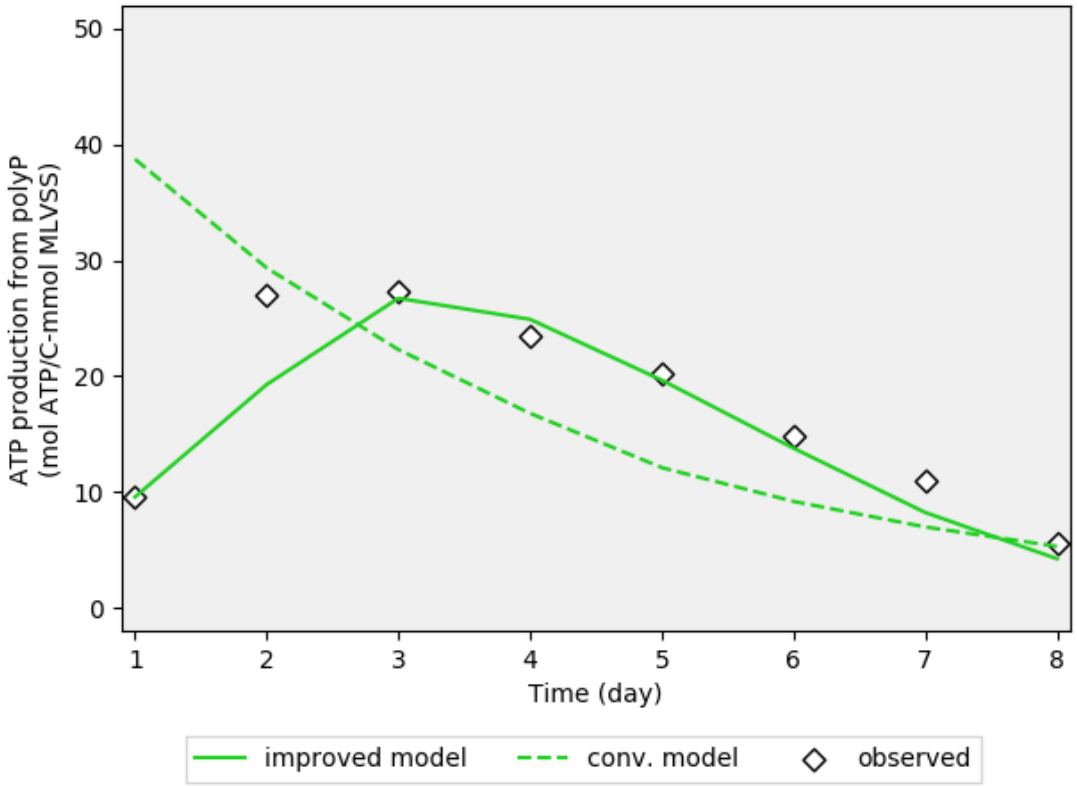

367

368 Figure 2. Comprison of model predictions and experimental observations of glycogen-contributed (top) and
369 polyP-contributed (bottom) ATP during an 8-day anaerobic starvation testing with acetate-fed lab-scale
370 EBPR system containing about 85% as Accumulibacter-PAOs (used as calibration dataset) by Lu et al.
371 (2007). The improved model (this study) is designed with sequential anaerobic maintenance polymer usage,
372 staged maintenance-decay and glycolysis-TCA pathway shift; iAlgae uses the same first-order decay as
373 ASM2 [34,56].

374 The staged maintenance-decay mechanism also predicts a different PAO biomass decay kinetics
375 from those by the traditional first-order model. An accelerating release of ammonia nitrogen was
376 observed in the experiments which accompanied with the deceleration of polyP release at the end
377 of Day 4. This indicates the PAO cells approached the depletion of both intracellular polymers and
378 started decay, as the nitrogen-containing substance began to lysis from dying cells as ammonia
379 [33,63]. The improved model captured the ammonia release acceleration by using the staged
380 maintenance-decay mechanism (Figure 1 top). The calibrated PAOs biomass decay rate was

381 0.007/d, being close to the reported value as 0.006/d as reported in original experiment. To predict
382 the same amount of biomass decay using the traditional constant first-order lysis mechanism, the
383 decay rate had to be calibrated to 0.0028/d (the dash line of NH_4^+-N in Figure 1 (top)), which is
384 53% less than the reported value. This inaccurate approximation of biomass decay when using
385 traditional model may potentially lead to either overestimating PAO biomass loss before their
386 polymer depletion or underestimating the PAOs' biomass loss after. This effect can have much
387 more impact on simulating processes with extended anaerobic incubation HRT such as in S2EBPR
388 system, therefore it is crucial to incorporate this mechanism in order to improve the modeling
389 performance of a variety of S2EBPR systems.

390 **Case study: Simulating PAO and GAO competition under prolonged anaerobic incubation**
391 **using Full-scale S2EBPR biomass**

392 **Model prediction at bulk level**

393 The calibrated model was used to simulate an independent anaerobic incubation batch testing
394 similar to the conditions in side-stream reactor in S2EBPR systems [64]. The testing sludge was
395 sampled from the side-stream fermentation reactor (SSR configuration) of South Cary Water
396 Reclamation Facility (Apex, North Carolina) as described by Nicholas et al. (2018) and Onnis-
397 Hayden et al. (2018) [9,64]. It was estimated to contain 6.9% biovolume as Accumulibacter-PAOs
398 and 1.1% as known GAOs by fluoresces in-situ hybridization (FISH) [64]. The batch test was
399 conducted as a 72-hour anaerobic incubation without external VFA feeding, and the residual
400 orthophosphate, residual VFA, MLSS glycogen and PHA were monitored and measured at 0, 6,
401 12, 18, 24, 36 and 72 hours after the beginning of this incubation. The model was fitted to these

temporal profiles with adjustment on initial status and biomass-composition-related parameters, including initial polymer contents, biomass concentration of all three species and the fraction of TCA-cycle-enabled agents in PAO species. In addition, OHOs' biomass decay rate was also adjusted to the experimentally identified value. All other kinetic and stoichiometric parameters were set identical to the lab-scale sludge calibration results, no more kinetic calibrations were conducted. GAOs' kinetic and stoichiometric parameters were set identical to PAOs' except the yield ratio of PHA to VFA uptake, since GAOs lack polyP and rely on glycogen to provide both ATP and reducing power in this process [2,7].

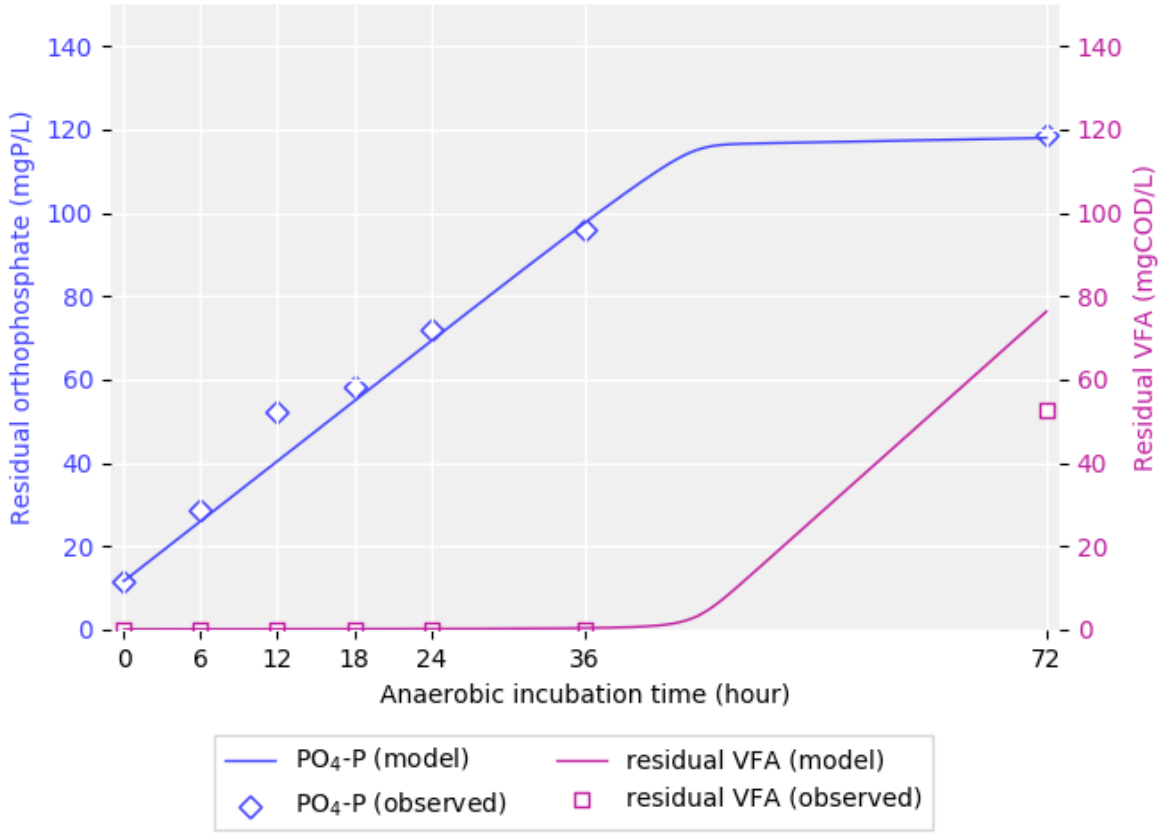

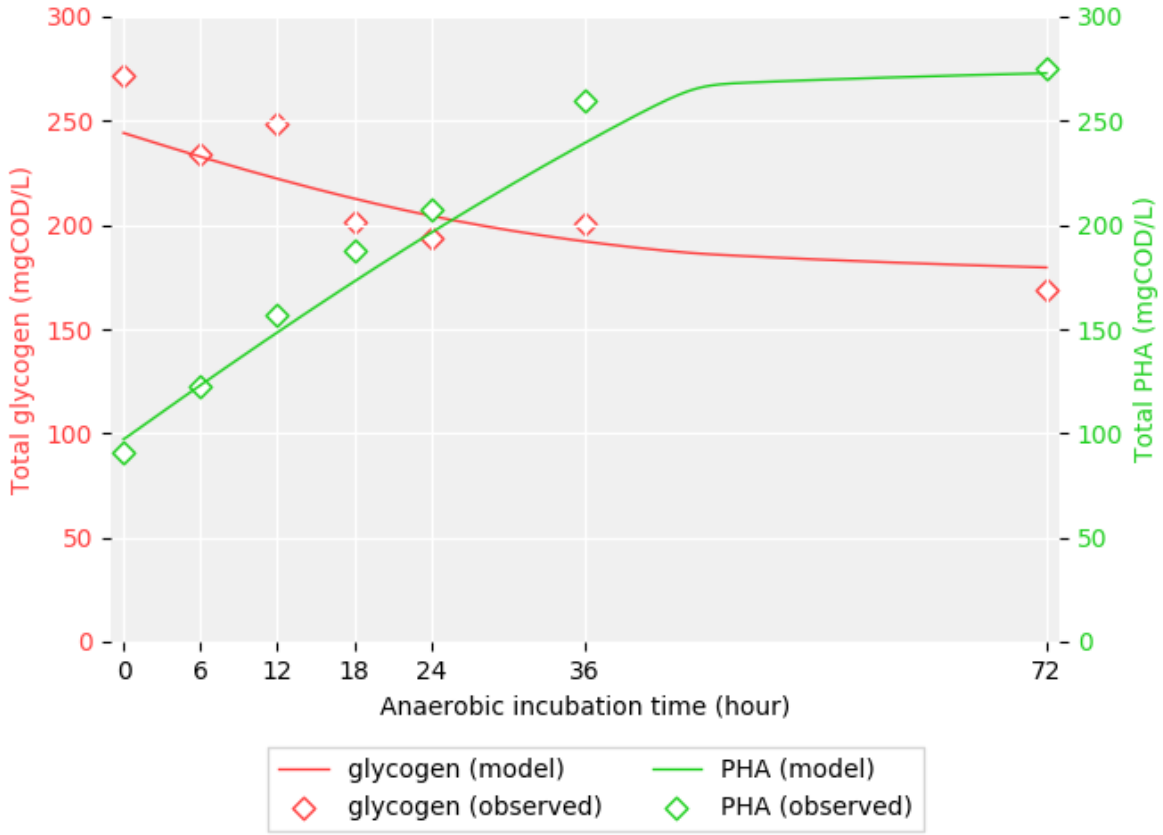

411

412 Figure 3. Comparison of experimental measurements with Simulated temporal trends of residual orthoP,
413 intracellular PHA and glycogen in a 72-hour anaerobic incubation batch test using sludge sampled from
414 full-scale S2EBPR system (SSR configuration, South Cary WRF, Apex, NC) estimated to contain 6.9% as
415 Accumulibacter-PAO, 1.1% as GAOs (by FISH, biovolume), using the improved model iEBPR that
416 incorporates sequential polymer utilization in cell maintenance, staged maintenance-decay and glycolysis-
417 TCA pathway shift. Top: residual orthophosphate and residual VFA; Bottom: MLSS glycogen and PHA.

418 Figure 3 shows the comparison of the observed measurements with the predicted temporal profiles
419 of residual PO_4-P, residual VFA, total MLSS PHA and glycogen during the anaerobic batch
420 testing. The OHO decay rate was calculated to be 0.0076/d based on the VFA requirement to fit
421 the observed stoichiometry of P release, glycogen consumed and PHA formation, since in this
422 model the hydrolysis and fermentation process is integrated into biomass decay. The simulated

423 residual PO_4-P, MLSS glycogen and PHA agreed well with observed data with RMSEs of
424 4.9mgP/L, 16.5mgCOD/L and 11.15 mgCOD/L respectively; the RMSE of residual VFA was
425 8.9mgCOD/L and about 22mgCOD/L VFA was overestimated by the model at 72 hours. The
426 model predicted a transitioning at around 45 hours from high-rate active P release with significant
427 PHA synthesis phase to a second phase with slower increase in both PHA and residual P.
428 Calculated yield ratio of the active P release to PHA formation from 36-72 hours was 1.77 mol-
429 P/C-mol PHA, which is higher than the typical range 0.36-0.77 mol-P/C-mol PHA for A/O
430 enriched sludge [4,30,36,47] and 0.78-1.22 mol-P/C-mol PHA for S2EBPR sludge [20]. This implies an
431 excessive source was contributing to the PO_4-P release which was not related to VFA uptake and
432 PHA formation, potentially being cell maintenance.

433 **Model prediction at cellular and population level**

434 However, investigate detailed polymer transformation at this bulk level is limited due to the lack
435 of resolution of real-time polymer distribution at population and cellular levels that better reflect
436 the competition between PAOs and GAOs , which may result in different metabolic patterns co-
437 exist according to the actual polymer storage in individual cells. To further validate the proposed
438 mechanism of polymer-dependent and staged maintenance and decay, SCRS was employed to
439 measure and reveal the intracellular polymer dynamics in PAOs and GAOs that ultimately dictates
440 their competition, and they were compared with the agent-based model results. The initial
441 distributions of PAOs' and GAOs' intracellular polymers namely polyP and glycogen in PAOs
442 and glycogen in GAOs, were adjusted manually after their means were determined in the previous
443 bulk-level step following the previous protocol [56]. Their temporal trends were represented by
444 snapshotting the modeled residue polymers across PAO/GAO species at 0, 6, 12, 24 36 and 72

hours, and were compared to the experimentally acquired distributions by SCRS at the same time points. [41,60,61]. As shown in Figure 4, the model accurately predicted the measurements at cellular and population levels, proving that the model mechanisms to be effective in modeling highly resolved PAO/GAO intracellular polymer metabolisms.

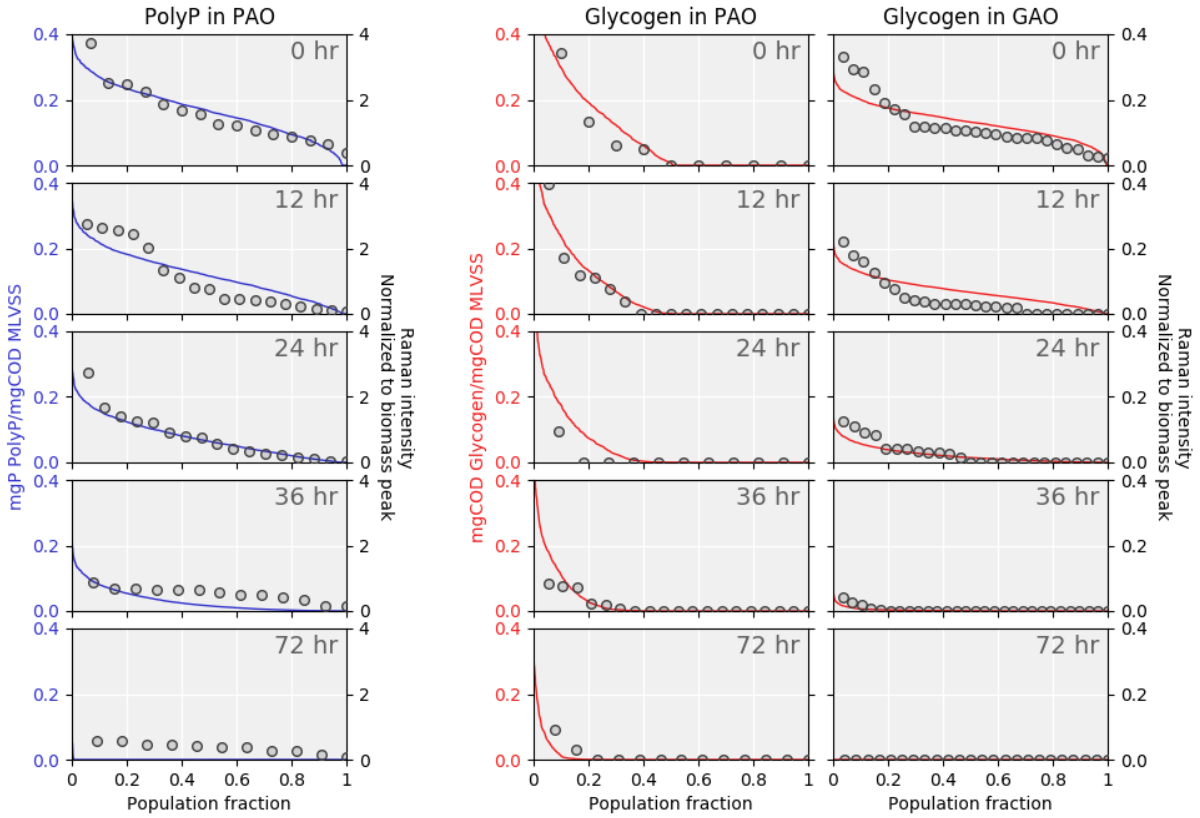

Figure 4. PAO polyP, glycogen and GAO glycogen in-species distribution by agent-based modeling (lines) and the actual distribution acquired by Raman single-cell microspectrascopy (dots) during a 72-hranaerobic incubation batch test (this study) with sludge sampled from full-scale S2EBPR system (SSR configuration, South Cary WRF, Apex, NC).

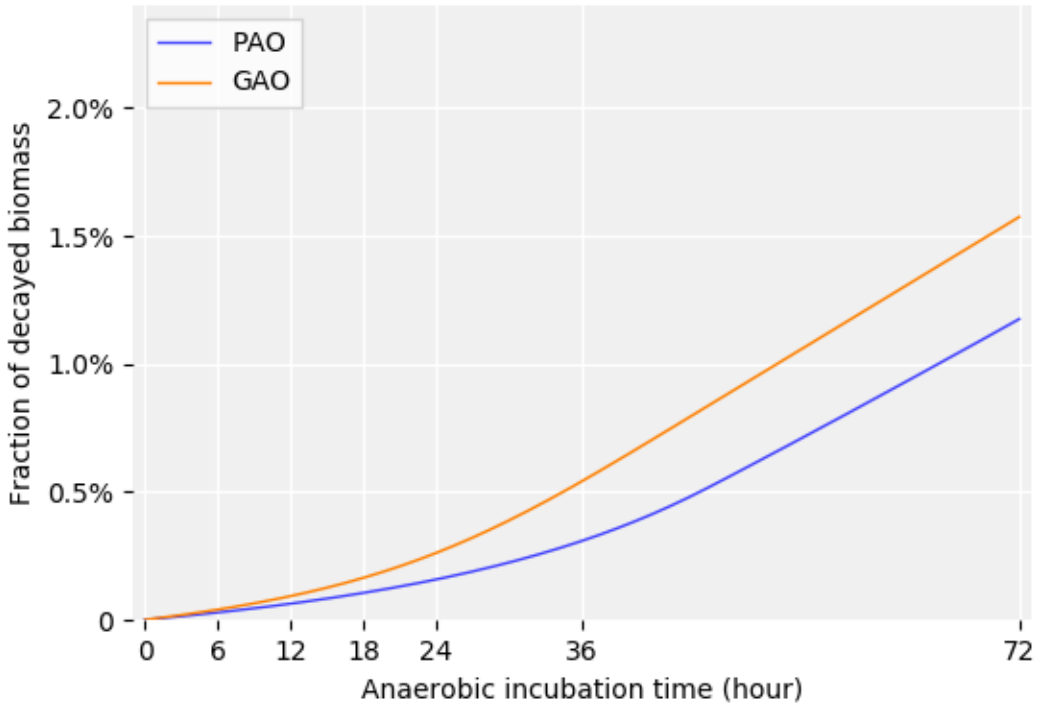

Figure 5. iEBPR predicted PAO and GAO decay based on sequential polymer utilization in cell maintenance and staged maintenance-decay mechanism of a 72-hour anaerobic incubation batch test using sludge sampled from full-scale S2EBPR system (SSR configuration, South Cary WRF, Apex, NC) estimated to contain 6.9% as Accumulibacter-PAO, 1.1% as GAOs (by FISH, biovolume). GAOs were speculated to have more cumulative biomass decay due to their earlier depletion of intracellular polymers. Agent-based modeling predicted slower and less PAOs decay than GAOs.

PAO-GAO competition. The SCRS dataset showed a clear 2-phase glycogen depletion trend in GAO cells: (1) an active utilization phase before 36 hours; (2) nearly depleted to a full depletion within 36-72 hours. The glycogen in PAOs showed a similar decreasing trend but a portion of the PAO cells contained detectable amount of glycogen up to 72 hours. In contrary to the faster depletion, GAO cells were estimated to contain higher initial glycogen contents. The mean available glycogen content in GAO cells was estimated to be 0.126 mgCOD/mgMLVSS COD, while was 0.098 mgCOD/mgMLVSS COD in PAO cells. This difference agreed with previous

468 studies suggesting that GAOs has a higher capability of glycogen storages [2,28,29,57]. The faster
469 depletion indicated that the GAOs have higher overall glycogen utilization rate than PAOs under
470 such conditions. The model identified this difference as an indication that the two independent
471 sources, polyP and glycogen, potentially provide larger amount of energy (ATP) anaerobically.
472 Hence PAOs may gain competitive advantage over GAOs for persisting a longer period of
473 maintenance under extended anaerobic conditions, and potentially start decay later and slower in
474 the first 36 hours of incubation (Figure 4, Figure 5). This differential decay rates in PAOs and
475 GAOs would likely contribute to the PAO's competitive advantage over GAOs under prolonged
476 anaerobic conditions. As a result, the staged maintenance-decay model predicted GAOs had 33%
477 more cumulative biomass decayed (1.6%) than PAOs (1.2%) during the 72-hr incubation (Figure
478 5). Meanwhile, the model predicted a complete depletion of polyP at 72 hours, which is consistent
479 with the relatively consistent residue polyP level in PAOs as revealed by the SCRS. This implies
480 a background amount of polyP potentially from non-PAO cells or "inert" polyP portion which is
481 not releasable [35].

482 ***Glycolysis-TCA pathway switch.*** SCRS data revealed that only about half of observed PAO
483 population contained glycogen at the beginning of this anaerobic incubation (Figure 4). Some of
484 the Accumulibacter-PAOs could have accumulated glycogen below SCRS detection limit, or there
485 were non-Accumulibacter-PAOs that had different metabolisms, for example, Tetrasphaera [65,66].
486 A comprehensive model for these non-Accumulibacter-PAOs is still under active exploration. In
487 addition, current knowledge assumes that PHA is always the final product of glycogen degradation
488 in Accumulibacter-PAOs' anaerobic metabolism [45,47]. Therefore assuming all PAOs being
489 Accumulibacter-PAOs may potentially lead to an over-prediction of overall PHA formation since
490 PHA is not synthesized by Tetrasphaera [65]. Under these assumptions, the model suggested that

491 almost all PAO cells in this case study can use TCA cycles to support PHA synthesis, and the
492 employment of TCA cycle was predicted to be at greater extent of involvement comparing to the
493 glycolysis-based metabolism. This was supported by the observed consistent, continuous P release
494 and PHA formation independent to the decreasing availability of glycogen. Detailed calculations
495 on the agent-based simulation results showed that PAOs had accumulated 0.20 C-mol VFA/C-mol
496 VSS by the end of 72 hours, which was significantly higher than GAOs VFA uptake, 0.61 C-mol
497 VFA/C-mol VSS. Using the stoichiometry of 0.22 mol NAD(P)H/C-mol VFA (TCA cycle) [43] and
498 0.33 mol NAD(P)H/C-mol VFA (using glycogen) [45], it is calculated that 59% of total reducing
499 power consumed in PAOs' PHA synthesis was provided from TCA cycle during the 72hr
500 incubation. This further indicates that under extended anaerobic phases as in S2EBPR, the PAOs
501 may gain competitive advantage over GAOs due to the possession of multiple intracellular
502 polymers and the adaptive switching of the anaerobic metabolic pathways.

503 The iEBPR agent-based model that incorporates the sequential polymer usage, staged
504 maintenance-decay processes and glycolysis-TCA pathway shift was developed, which was
505 calibrated and validated using both bulk batch test experimental data and high-resolution cellular
506 and population-level measurements enabled by SCRS. These newly proposed model modifications
507 are expected to improve the simulation accuracy on S2EBPR systems, particularly SSR (side-
508 stream RAS fermentation) and SSRC (SSR with carbon addition) configurations where a longer
509 anaerobic S2EBPR SRT may lead to the manifestation of more complicated PAO/GAO
510 competition metabolisms that differ from those in play in conventional EBPR systems (i.e. A2O
511 configuration). The model revealed that under extended anaerobic phases as in S2EBPR, the PAOs
512 may gain competitive advantage over GAOs due to the possession of multiple intracellular
513 polymers and the adaptive switching of the anaerobic metabolic pathways that consequently lead

514 to longer maintenance period prior to the later and slower decay in PAOs compared with shorter
515 maintenance period before the earlier and faster decay in GAOs. The iEBPR model can be applied
516 to facilitate and optimize the design and operations of S2EBPR for more reliable nutrient removal
517 and recovery from wastewater.

518 **REFERENCES**

519 (1) Gu, A. Z.; Tooker, N. B.; Onnis-Hayden, A.; Wang, D.; Li, G.; Srinivasan, V.; Takács, I.
520 *Investigation of the Mechanisms for Optimization and Design of a Side-Stream EBPR*
521 *Process as a Sustainable Approach for Achieving Stable and Efficient Phosphorus*
522 *Removal*.; WE&RF, 2018.
523 (2) Zeng, R. J.; van Loosdrecht, M.; Yuan, Z.; Keller, J. Metabolic Model for Glycogen-
524 accumulating Organisms in Anaerobic/Aerobic Activated Sludge Systems. *Biotechnol.*
525 *Bioeng*. **2003**, *81* (1), 92–105.
526 (3) Oehmen, A.; Zeng, R. J.; Saunders, A. M.; Blackall, L. L.; Keller, J.; Yuan, Z. Anaerobic
527 and Aerobic Metabolism of Glycogen-Accumulating Organisms Selected with Propionate
528 as the Sole Carbon Source. *Microbiology* **2006**, *152* (9), 2767–2778.
529 (4) Smolders, G.; Van der Meij, J.; Van Loosdrecht, M.; Heijnen, J. Model of the Anaerobic
530 Metabolism of the Biological Phosphorus Removal Process: Stoichiometry and PH
531 Influence. *Biotechnol. Bioeng*. **1994**, *43* (6), 461–470.
532 (5) Gu, A. Z.; Saunders, A.; Neethling, J.; Stensel, H.; Blackall, L. Functionally Relevant
533 Microorganisms to Enhanced Biological Phosphorus Removal Performance at Full-Scale
534 Wastewater Treatment Plants in the United States. *Water Environ. Res*. **2008**, *80* (8), 688–
535 698.
536 (6) Neethling, J.; Bakke, B.; Benisch, M.; Gu, A.; Stephens, H.; Stensel, H. D.; Moore, R.
537 *Factors Influencing the Reliability of Enhanced Biological Phosphorus Removal*; Water
538 Environment Research Foundation, 2006.
539 (7) Lopez-Vazquez, C. M.; Oehmen, A.; Hooijmans, C. M.; Brdjanovic, D.; Gijzen, H. J.; Yuan,
540 Z.; van Loosdrecht, M. C. Modeling the PAO–GAO Competition: Effects of Carbon Source,
541 PH and Temperature. *Water Res*. **2009**, *43* (2), 450–462.
542 (8) Majed, N.; Gu, A. Z. Insights into the Metabolic Pathways and Diversity of Functionally
543 Relevant Populations in Enhanced Biological Phosphorus Removal Processes Using Raman
544 Microscopy. *Proc. Water Environ. Fed*. **2011**, *2011* (11), 4824–4832.
545 (9) Onnis-Hayden, A.; Tooker, N.; Srinivasan, V.; Gu, A. Survey of Plants Operating in Side-
546 Stream EBPR Mode and Comparison with Conventional: Process Stability, Kinetics and
547 Microbial Population (in Review).
548 (10) Nielsen, P. H.; McIlroy, S. J.; Albertsen, M.; Nierychlo, M. Re-Evaluating the Microbiology
549 of the Enhanced Biological Phosphorus Removal Process. *Curr. Opin. Biotechnol*. **2019**,
550 *57*, 111–118.
551 (11) Wang, D.; Tooker, N. B.; Srinivasan, V.; Li, G.; Fernandez, L. A.; Schauer, P.; Menniti, A.;
552 Maher, C.; Bott, C. B.; Dombrowski, P.; Barnard, J. L.; Onnis-Hayden, A.; Gu, A. Z. Side-
553 Stream Enhanced Biological Phosphorus Removal (S2EBPR) Process Improves System

Performance - A Full-Scale Comparative Study. *Water Res*. **2019**, *167*, 115109. https://doi.org/10.1016/j.watres.2019.115109.

(12) Barnard, J.; Abraham, K. Key Features of Successful BNR Operation. *Water Sci. Technol*. **2006**, *53* (12), 1–9.

(13) Barnard, J.; Houweling, D.; Analla, H.; Steichen, M. Fermentation of Mixed Liquor for Phosphorus Removal. *Proc. Water Environ. Fed*. **2010**, *2010* (18), 59–71.

(14) Stevens, G.; Ellsworth, A.; Wyman, M.; Lambrecht, A. BNR Process Using RAS Anaerobic Zone. *Proc. Water Environ. Fed*. **2015**, *2015* (3), 1–3.

(15) Stroud, R.; Martin, C. South Cary Water Reclamation Facility's Nutrient Removal Modifications and Reduction Success, Town of Cary, North Carolina. *Proc. Water Environ. Fed*. **2001**, *2001* (14), 337–345.

(16) Copp, J. B.; Belk, I.; Vale, P. Operational Control of a RAS Fermentation Process for Enhancing Biological Phosphorus Removal. *Proc. Water Environ. Fed*. **2012**, *2012* (9), 6056–6068.

(17) Vale, P.; Barnard, J.; Thomas, D.; Dold, P. RAS Fermentation to Enhance Biological Phosphorus Removal. In *Proceedings of the WEFTEC Conference*; 2008.

(18) Vollertsen, J.; Petersen, G.; Borregaard, V. R. Hydrolysis and Fermentation of Activated Sludge to Enhance Biological Phosphorus Removal. *Water Sci. Technol*. **2006**, *53* (12), 55–64.

(19) Srinivasan, V. N.; Li, G.; Wang, D.; Tooker, N. B.; Dai, Z.; Onnis-Hayden, A.; Pinto, A.; Gu, A. Z. Oligotyping and Genome-Resolved Metagenomics Reveal Distinct Candidatus Accumulibacter Communities in Full-Scale Side-Stream versus Conventional Enhanced Biological Phosphorus Removal (EBPR) Configurations. *bioRxiv* **2019**, 596692.

(20) Lanham, A. B.; Oehmen, A.; Saunders, A. M.; Carvalho, G.; Nielsen, P. H.; Reis, M. A. Metabolic Versatility in Full-Scale Wastewater Treatment Plants Performing Enhanced Biological Phosphorus Removal. *Water Res*. **2013**, *47* (19), 7032–7041.

(21) Mielczarek, A. T.; Nguyen, H. T. T.; Nielsen, J. L.; Nielsen, P. H. Population Dynamics of Bacteria Involved in Enhanced Biological Phosphorus Removal in Danish Wastewater Treatment Plants. *Water Res*. **2013**, *47* (4), 1529–1544.

(22) Stokholm-Bjerregaard, M.; McIlroy, S. J.; Nierychlo, M.; Karst, S. M.; Albertsen, M.; Nielsen, P. H. A Critical Assessment of the Microorganisms Proposed to Be Important to Enhanced Biological Phosphorus Removal in Full-Scale Wastewater Treatment Systems. *Front. Microbiol*. **2017**, *8*, 718.

(23) Dunlap, P.; Martin, K.; Stevens, G.; Tooker, N.; Barnard, J.; Gu, A.; Takacs, I.; Shaw, A.; Onnis-Hayden, A.; Li, Y. Rethinking EBPR: What Do You Do When the Model Will Not Fit Real-World Evidence? 5th IWA. In *WEF Wastewater Treatment Modeling Seminar, Annecy, France*; 2016; pp 39–62.

(24) Houweling, D.; Comeau, Y.; Takács, I.; Dold, P. Uncertainty and Variability in Enhanced Biological Phosphorus Removal (EBPR) Stoichiometry: Consequences for Process Modelling and Optimization. *Water Sci. Technol*. **2010**, *61* (7), 1793–1800.

(25) da Silva, L. G.; Gamez, K. O.; Gomes, J. C.; Akkermans, K.; Welles, L.; Abbas, B.; van Loosdrecht, M. C.; Wahl, S. A. Revealing Metabolic Flexibility of Candidatus Accumulibacter Phosphatis through Redox Cofactor Analysis and Metabolic Network Modeling. *bioRxiv* **2018**, 458331.

(26) Li, G.; Tooker, N. B.; Wang, D.; Srinivasan, V.; Barnard, J. L.; Schauer, P.; Takács, I.; Onnis-Hayden, A.; Gu, A. Z. Application of Agent-Based Modeling to Reveal Competition

between PAOs and GAOs in Side-Stream EBPR (S2EBPR) Systems. *Proc. Water Environ. Fed.* **2018**, *2018* (5), 269–274.

(27) Wentzel, M.; Dold, P.; Ekama, G.; Marais, G. Enhanced Polyphosphate Organism Cultures in Activated Sludge Systems. Part III: Kinetic Model. *Water A* **1989**, *15* (2), 89–102.

(28) Mino, T.; Van Loosdrecht, M.; Heijnen, J. Microbiology and Biochemistry of the Enhanced Biological Phosphate Removal Process. *Water Res.* **1998**, *32* (11), 3193–3207.

(29) Vargas, M.; Yuan, Z.; Pijuan, M. Effect of Long-Term Starvation Conditions on Polyphosphate-and Glycogen-Accumulating Organisms. *Bioresour. Technol.* **2013**, *127*, 126–131.

(30) Filipe, C. D.; Daigger, G. T.; Grady, C. Effects of PH on the Rates of Aerobic Metabolism of Phosphate-Accumulating and Glycogen-Accumulating Organisms. *Water Environ. Res.* **2001**, *73* (2), 213–222.

(31) Filipe, C. D.; Daigger, G. T.; Grady, C. A Metabolic Model for Acetate Uptake under Anaerobic Conditions by Glycogen Accumulating Organisms: Stoichiometry, Kinetics, and the Effect of PH. *Biotechnol. Bioeng.* **2001**, *76* (1), 17–31.

(32) Lopez, C.; Pons, M.; Morgenroth, E. Endogenous Processes during Long-Term Starvation in Activated Sludge Performing Enhanced Biological Phosphorus Removal. *Water Res.* **2006**, *40* (8), 1519–1530.

(33) Lu, H.; Keller, J.; Yuan, Z. Endogenous Metabolism of Candidatus Accumulibacter Phosphatis under Various Starvation Conditions. *Water Res.* **2007**, *41* (20), 4646–4656.

(34) Henze, M.; Harremoes, P.; la Cour Jansen, J.; Arvin, E. *Wastewater Treatment: Biological and Chemical Processes*; Springer Science & Business Media, 2001.

(35) Barker, P.; Dold, P. General Model for Biological Nutrient Removal Activated-Sludge Systems: Model Presentation. *Water Environ. Res.* **1997**, *69* (5), 969–984.

(36) Hu, Z.; Wentzel, M.; Ekama, G. A General Kinetic Model for Biological Nutrient Removal Activated Sludge Systems: Model Development. *Biotechnol. Bioeng.* **2007**, *98* (6), 1242–1258.

(37) Lanham, A. B.; Oehmen, A.; Saunders, A. M.; Carvalho, G.; Nielsen, P. H.; Reis, M. A. Metabolic Modelling of Full-Scale Enhanced Biological Phosphorus Removal Sludge. *Water Res.* **2014**, *66*, 283–295.

(38) Santos, J. M.; Rieger, L.; Lanham, A. B.; Carvalheira, M.; Reis, M. A.; Oehmen, A. A Novel Metabolic-ASM Model for Full-Scale Biological Nutrient Removal Systems. *Water Res.* **2020**, *171*, 115373.

(39) Hauduc, H.; Rieger, L.; Oehmen, A.; Van Loosdrecht, M.; Comeau, Y.; Héduit, A.; Vanrolleghem, P.; Gillot, S. Critical Review of Activated Sludge Modeling: State of Process Knowledge, Modeling Concepts, and Limitations. *Biotechnol. Bioeng.* **2013**, *110* (1), 24–46.

(40) Li, G.; Tooker, N. B.; Wang, D.; Srinivasan, V.; Onnis-Hayden, A.; Barnard, J. L.; Russel, A.; Bott, C. B.; Schauer, P.; Dombrowski, P.; Shaw, A.; Stinson, B.; Stevens, G.; Dunlap, P.; Phillips, H.; Analla, H.; Lambrecht, A.; McQuarrie, J.; Takács, I.; Gu, A. Z. Modeling Side-Stream Enhanced Biological Phosphorus Removal (S2EBPR) Systems: Insights from Versatile Anaerobic Pathways. *Proc. Water Environ. Fed.* **2020**.

(41) Majed, N.; Matthäus, C.; Diem, M.; Gu, A. Z. Evaluation of Intracellular Polyphosphate Dynamics in Enhanced Biological Phosphorus Removal Process Using Raman Microscopy. *Environ. Sci. Technol.* **2009**, *43* (14), 5436–5442.

(42) Mino, T.; Arun, V.; Tsuzuki, Y.; Matsuo, T. Effect of Phosphorus Accumulation on Acetate Metabolism in the Biological Phosphorus Removal Process. In *Biological phosphate removal from wastewaters*; Elsevier, 1987; pp 27–38.
(43) Comeau, Y.; Hall, K.; Hancock, R.; Oldham, W. Biochemical Model for Enhanced Biological Phosphorus Removal. *Water Res*. **1986**, *20* (12), 1511–1521.
(44) Maurer, M.; Gujer, W.; Hany, R.; Bachmann, S. Intracellular Carbon Flow in Phosphorus Accumulating Organisms from Activated Sludge Systems. *Water Res*. **1997**, *31* (4), 907–917.
(45) Zhou, Y.; Pijuan, M.; Zeng, R. J.; Yuan, Z. Involvement of the TCA Cycle in the Anaerobic Metabolism of Polyphosphate Accumulating Organisms (PAOs). *Water Res*. **2009**, *43* (5), 1330–1340.
(46) Pereira, H.; Lemos, P. C.; Reis, M. A.; Crespo, J. P.; Carrondo, M. J.; Santos, H. Model for Carbon Metabolism in Biological Phosphorus Removal Processes Based on in Vivo13C-NMR Labelling Experiments. *Water Res*. **1996**, *30* (9), 2128–2138.
(47) Yagci, N.; Artan, N.; Çokgör, E. U.; Randall, C. W.; Orhon, D. Metabolic Model for Acetate Uptake by a Mixed Culture of Phosphate-and Glycogen-Accumulating Organisms under Anaerobic Conditions. *Biotechnol. Bioeng*. **2003**, *84* (3), 359–373.
(48) Pijuan, M.; Oehmen, A.; Baeza, J. A.; Casas, C.; Yuan, Z. Characterizing the Biochemical Activity of Full-Scale Enhanced Biological Phosphorus Removal Systems: A Comparison with Metabolic Models. *Biotechnol. Bioeng*. **2008**, *99* (1), 170–179.
(49) Brdjanovic, D.; van Loosdrecht, M. C.; Hooijmans, C. M.; Mino, T.; Alaerts, G. J.; Heijnen, J. J. Bioassay for Glycogen Determination in Biological Phosphorus Removal Systems. *Water Sci. Technol*. **1998**, *37* (4–5), 541–547.
(50) Hesselmann, R.; Von Rummell, R.; Resnick, S. M.; Hany, R.; Zehnder, A. Anaerobic Metabolism of Bacteria Performing Enhanced Biological Phosphate Removal. *Water Res*. **2000**, *34* (14), 3487–3494.
(51) He, S.; McMahon, K. D. 'Candidatus Accumulibacter'Gene Expression in Response to Dynamic EBPR Conditions. *ISME J*. **2011**, *5* (2), 329.
(52) Wilmes, P.; Wexler, M.; Bond, P. L. Metaproteomics Provides Functional Insight into Activated Sludge Wastewater Treatment. *PLoS One* **2008**, *3* (3), e1778.
(53) Schuler, A. J.; Jenkins, D. Enhanced Biological Phosphorus Removal from Wastewater by Biomass with Different Phosphorus Contents, Part III: Anaerobic Sources of Reducing Equivalents. *Water Environ. Res*. **2003**, *75* (6), 512–522.
(54) Brdjanovic, D.; Van Loosdrecht, M.; Hooijmans, C.; Mino, T.; Alaerts, G.; Heijnen, J. Effect of Polyphosphate Limitation on the Anaerobic Metabolism of Phosphorus-Accumulating Microorganisms. *Appl. Microbiol. Biotechnol*. **1998**, *50* (2), 273–276.
(55) Martín, H. G.; Ivanova, N.; Kunin, V.; Warnecke, F.; Barry, K. W.; McHardy, A. C.; Yeates, C.; He, S.; Salamov, A. A.; Szeto, E.; others. Metagenomic Analysis of Two Enhanced Biological Phosphorus Removal (EBPR) Sludge Communities. *Nat. Biotechnol*. **2006**, *24* (10), 1263.
(56) Bucci, V.; Majed, N.; Hellweger, F. L.; Gu, A. Z. Heterogeneity of Intracellular Polymer Storage States in Enhanced Biological Phosphorus Removal (EBPR)–Observation and Modeling. *Environ. Sci. Technol*. **2012**, *46* (6), 3244–3252.
(57) Smolders, G.; Klop, J.; Van Loosdrecht, M.; Heijnen, J. A Metabolic Model of the Biological Phosphorus Removal Process: I. Effect of the Sludge Retention Time. *Biotechnol. Bioeng*. **1995**, *48* (3), 222–233.

(58) Acevedo, B.; Oehmen, A.; Carvalho, G.; Seco, A.; Borrás, L.; Barat, R. Metabolic Shift of Polyphosphate-Accumulating Organisms with Different Levels of Polyphosphate Storage. *Water Res*. **2012**, *46* (6), 1889–1900. https://doi.org/10.1016/j.watres.2012.01.003.

(59) Smolders, G.; Van der Meij, J.; Van Loosdrecht, M.; Heijnen, J. Stoichiometric Model of the Aerobic Metabolism of the Biological Phosphorus Removal Process. *Biotechnol. Bioeng*. **1994**, *44* (7), 837–848.

(60) Majed, N.; Gu, A. Z. Application of Raman Microscopy for Simultaneous and Quantitative Evaluation of Multiple Intracellular Polymers Dynamics Functionally Relevant to Enhanced Biological Phosphorus Removal Processes. *Environ. Sci. Technol*. **2010**, *44* (22), 8601–8608.

(61) Li, Y.; Cope, H. A.; Rahman, S. M.; Li, G.; Nielsen, P. H.; Elfick, A.; Gu, A. Z. Toward Better Understanding of EBPR Systems via Linking Raman-Based Phenotypic Profiling with Phylogenetic Diversity. *Environ. Sci. Technol*. **2018**, *52* (15), 8596–8606.

(62) Majed, N.; Gu, A. Z. Phenotypic Dynamics in Polyphosphate and Glycogen Accumulating Organisms in Response to Varying Influent C/P Ratios in EBPR Systems. *Sci. Total Environ*. **2020**, *743*, 140603.

(63) Gujer, W. *The Activated Sludge Model No. 2: Biological Phosphorus Removal: Proceedings IAWQ Specialised Seminar: Modelling and Control of Activated Sludge Processes, 22.-24. August 1994, Copenhagen*; IAWQ, 1994.

(64) Tooker, N.; Li, G.; Srinivasan, V.; Onnis-Hayden, A.; Gu, A. Elucidating the Mechanisms of Side-Stream Enhanced Biological Phosphorus Removal (in Review).

(65) Kristiansen, R.; Nguyen, H. T. T.; Saunders, A. M.; Nielsen, J. L.; Wimmer, R.; Le, V. Q.; McIlroy, S. J.; Petrovski, S.; Seviour, R. J.; Calteau, A.; others. A Metabolic Model for Members of the Genus Tetrasphaera Involved in Enhanced Biological Phosphorus Removal. *ISME J*. **2013**, *7* (3), 543.

(66) Fernando, E. Y.; McIlroy, S. J.; Nierychlo, M.; Herbst, F.-A.; Petriglieri, F.; Schmid, M. C.; Wagner, M.; Nielsen, J. L.; Nielsen, P. H. Resolving the Individual Contribution of Key Microbial Populations to Enhanced Biological Phosphorus Removal with Raman–FISH. *ISME J*. **2019**, 1.